Applied Catalysis B: Environmental 152–153 (2014) 108–116

Contents lists available at ScienceDirect

Applied Catalysis B: Environmental

journal homepage: www.elsevier.com/locate/apcatb

Experimental and kinetic study of SO_2 oxidation on a Pt/γ-Al_2O_3 catalyst

Tayebeh Hamzehlouyan[a], Chaitanya Sampara[a], Junhui Li[b], Ashok Kumar[b], William Epling[a,*]

[a] Department of Chemical and Biomolecular Engineering, University of Houston, Houston, TX, United States
[b] Catalyst Technology, Cummins Inc., Columbus, IN, United States

ARTICLE INFO

Article history:
Received 15 October 2013
Received in revised form 3 January 2014
Accepted 4 January 2014
Available online 25 January 2014

Keywords:
SO_2 oxidation
Oxidation catalysis
Sulfur poisoning

ABSTRACT

An SO_2 oxidation experimental study was performed and a kinetic model was developed to describe SO_2 oxidation over a Pt/γ-Al_2O_3 oxidation catalyst. An apparent activation energy of 98.8 kJ mol^{-1} was measured when SO_3 was present in the feed. Reaction orders of 0.88 and −0.24 were obtained for SO_2 and O_2, respectively, and the SO_3 reaction order was found to be −0.42. A microkinetic model based on a Langmuir-Hinshelwood mechanism was proposed and a one dimensional steady-state model was developed. A plug flow reactor model was assumed and the set of algebraic differential equations was solved at various temperatures to predict the SO_2 conversion as a function of temperature. The relative importance of each step in the reaction mechanism was studied at different temperatures to identify the rate determining step (RDS). According to the model, at temperatures below 300 °C, O_2 adsorption/desorption and the surface reaction between the adsorbed SO_2 and oxygen control the overall rate, whereas at higher temperatures the surface reaction is the RDS. The model predictions imply that, at low temperatures, SO_3 inhibits SO_2 oxidation through occupation of the active sites required for oxygen adsorption, verifying the higher activation energy observed in the presence of SO_3 in the feed. The modeling results revealed that the relative importance of the individual rates in the mechanism as well as the surface coverages were strongly temperature dependent.

1. Introduction

Sulfur is a common poison for automotive catalysts. For example, sulfur oxides in diesel engine exhaust interact with the diesel oxidation catalyst (DOC) as well as other aftertreatment catalysts leading to performance loss over time [1]. A number of studies have focused on sulfur interactions with DOCs [1–3] and its effect on NO oxidation activity [4–6] and oxidation of other emissions [7,8]. In those investigations, sulfur interactions with the metal, metal oxides, as well as the catalyst support have been studied using experimental and computational methods. However, few studies have focused on the SO_2 oxidation reaction itself. DOC SO_2 oxidation kinetics would of course enable prediction of residual SO_2 and product SO_3 concentrations exiting the catalyst, which in turn could be used to determine deactivation rates of downstream catalyst systems.

Modeling of SO_2 interactions with Pt-based catalysts has been studied, however, mostly for lean NO_x trap (LNT, or NO_x storage/reduction (NSR)) catalysis in terms of diesel automotive applications. Olsson et al. [9] studied sulfur poisoning and regeneration of a Pt-containing LNT. They developed a kinetic model that included sulfur deactivation of the LNT, which accounted for sulfur poisoning, regeneration of the catalyst for NO_x trapping and sulfur release. Their sulfur sub-model contained steps for SO_2 adsorption on two sites, barium and alumina, and the subsequent oxidation to form sulfates. It was suggested that sulfur poisoning might occur on both Ba and alumina, with the poisoned Ba sites leading to NO_x storage loss [9]. Dawody et al. [10] studied the effect of SO_2 exposure conditions on sulfur accumulation on Pt/SiO_2 as well as its impact on the NO_x storage/reduction performance of a Pt/BaO/Al_2O_3 LNT and BaO/Al_2O_3. It was found that both SO_2 exposure in combination with O_2 or H_2 caused deactivation of the NO_x storage capacity of the NSR samples, but they noted that exposure to SO_2 with H_2 increased the formation of sulfur-containing species on the samples. Moreover, it was shown that the presence of Pt enhanced the adsorption of SO_2 under all exposure conditions [10]. In another study performed by Dawody et al. [11], a kinetic model was developed that included SO_2 interactions with a NSR catalyst. The model consisted of six sub-models: (i) NO_x storage under sulfur-free conditions; (ii) SO_2 storage on NO_x storage sites; (iii) SO_2 oxidation over platinum sites; (iv) SO_3 storage as bulk sulfates on both barium and alumina bulk sites; (v) SO_2 interaction

* Corresponding author. Tel.: +1 713 743 4234.
E-mail address: wsepling@uh.edu (W. Epling).

0926-3373/$ – see front matter © 2014 Elsevier B.V. All rights reserved.
http://dx.doi.org/10.1016/j.apcatb.2014.01.005

Nomenclature

a_j	active site density for reaction j (mol site m^{-3})
A	face area (m^2)
$\vec{c}_s$	vector of molar concentrations of trace species at catalyst surface (mol m^{-3})
F	function to specify surface coverages (s^{-1})
$k_{m,i}$	mass transfer coefficient for species i (mol m^{-2} s^{-1})
r_j	rate of production of reaction j (mol mol site^{-1} s^{-1})
s_{ij}	stoichiometric coefficient of species i in reaction j
S	surface area per reactor volume (m^{-1})
t	time (s)
T_g	temperature of bulk gas phase (K)
T_s	temperature of solid phase (K)
w	molar flow rate (mol s^{-1})
$x_{g,i}$	mole fraction of species i in bulk gas phase
$x_{s,i}$	mole fraction of species i in gas at catalyst surface
X_{SO_2}	outlet SO_2 conversion (%)
z	axial position (m)
$\vec{\theta}$	vector of surface coverages

with platinum in the presence of H_2; and (vi) oxidation of accumulated sulfur compounds on platinum by NO_2. Their model was able to describe the main features in the experiments such as the decrease in the NO_x storage performance after exposure to sulfur.

Many research groups have studied SO_2 oxidation over vanadium-based catalysts [12–16], with fewer evaluating Pt-based catalysts, however, these investigations mainly focus on SO_2 oxidation under conditions applicable to sulfuric acid production, i.e. with high concentrations of SO_2 (percent levels), and not those relevant to automotive emissions (ppm levels). For example, Benzinger et al. [17] investigated SO_2 oxidation kinetics over Pt in a micro-structured reactor. They performed a detailed mechanistic study and numerically simulated SO_3 formation in a single channel configuration. Good agreement was observed between their simulation results and the experimental data. A rate determining step sensitivity analysis on the reaction steps showed that the adsorption/desorption of SO_2 and the surface reaction between the adsorbed species were similar under their experimental conditions. Therefore, they suggested that the rate determining step could change depending on the experimental conditions. In work performed by Sharma et al. [18], a microkinetic model for SO_2 oxidation on Pt was proposed with an ultimate goal of understanding the DOC–SO_x interactions. They considered 12 reversible catalytic reactions and five surface species (S^*, O^*, SO^*, $SO_2{}^*$ and $SO_3{}^*$) with some kinetic parameters taken from the literature and some calculated using semi-empirical methods. Steady-state isothermal PFR simulations were performed and the model predictions were compared to the experimental data of a Pt/SiO_2 coated monolith. Two kinetic parameters were adjusted in their model and a further validation was carried out against SO_2 conversion experimental data with a Pt/TiO_2 catalyst. Fair agreement between the model predictions and experimental data was observed. The reversible surface reaction between the adsorbed species was identified as the most important reaction step based on their sensitivity analysis. However, SO_3 adsorption/desorption showed the largest sensitivity at low temperatures (250 °C) [18].

SO_2 adsorption on a Pt(1 1 1) surface and reactivity of the adsorbed sulfur species has been widely studied using different spectroscopic techniques [6,19–24]. First principles density functional study regarding SO_2 binding and oxidation on Pt has also been performed [25–27]. Lin et al. [25] performed DFT calculations and predicted that on an O precovered Pt(1 1 1) surface, the activation barrier for an assumed Eley-Rideal mechanism was less than that for the Langmuir-Hinshelwood reaction. However, they suggested that the actual mechanism of sulfur oxidation might be highly sensitive to environmental conditions due to the large sensitivity of the surface thermodynamics to oxygen coverage on Pt as well as the stability of surface-bound SO_4 under highly oxidizing conditions [25].

In the present work, a SO_2 oxidation model was built using data obtained from experiments with a monolithic Pt/γ-Al_2O_3 catalyst. As a starting point in developing the kinetic model, the kinetic scheme presented in Dawody et al. [11] was assumed. A systematic optimization methodology, previously reported in the literature [28], was used to estimate the rate coefficients using experimental data. A separate set of experimental data was used to verify the accuracy of the model. The relative importance of each step in the reaction mechanism was evaluated at different temperatures to identify the rate determining step (RDS).

2. Experimental methodology

2.1. Catalyst and reactor descriptions

The Pt/γ-Al_2O_3 catalyst used in this study was provided by Johnson Matthey in monolithic form. The monolith had a platinum loading of 50 g/ft^3, an Al_2O_3 loading of ~1.6 g/in^3, and a cell density of 325 channels/in^2. A monolithic core of 1.96 cm diameter and 3.68 cm length with a cross section of 130 cells was used in the bench reactor experiments. High temperature insulation was wrapped around the sample in order to block the space between the monolith and the wall of the reactor to minimize the gas flow bypassing the catalyst. The catalyst sample was inserted into a quartz tube reactor and small glass tubes, 2.5 mm i.d. and 3 mm o.d., were placed upstream of the sample to ensure mixing and uniformity of the gas flow. The reactor assembly was placed in a temperature controlled furnace. For temperature measurements, three thermocouples were inserted at different locations inside the reactor. One thermocouple was located upstream of the catalyst, the two others were placed inside the sample, one close to the inlet face and the other close to the outlet face, all radially centered. MKS mass flow controllers were used to meter the gas flow rates and to set the desired gas concentrations. The inlet and outlet gas lines were heated to 150–200 °C in order to enhance temperature uniformity of the monolith and to prevent deposition of sulfur species in the lines. For experiments that required SO_3 in the feed, SO_2 and O_2, were metered into an upstream reactor which consisted of another monolith core of Pt/γ-Al_2O_3. This catalyst was loaded in a 1 in diameter stainless steel tube reactor which was placed in a ceramic heater. A low flow rate, 300 ml/min with a space velocity of 3700 h^{-1} along with a relatively high temperature, i.e. in the range of 350–400 °C, were used such that complete conversion of SO_2 to SO_3 was achieved. An appropriate concentration of SO_2, balanced in O_2, was selected according to the desired SO_3 concentration in the main reactor, and metered through the catalyst core. This upstream reactor outlet was then added to the main feed stream and fed to the quartz tube reactor.

A MKS MultiGas MG-2030 FT-IR analyzer was used for the gas phase concentration measurements. The instrument was set to measure a data point every 0.5 s at a resolution of 0.5 cm^{-1}. Due to the interfering peaks of SO_2 and SO_3 in the IR absorption spectra, an accurate calibration method needed to be used for the SO_2 and SO_3 measurements. This calibration method was created by removing the overlapping regions of the SO_2 and SO_3 IR absorption spectra from the analysis band which is used for their quantification. Frequency ranges of 1294–1363 cm^{-1} and 1389–1426 cm^{-1} were selected as analysis bands in the SO_2 and SO_3 calibration meth-

ods, respectively, to minimize the effect of interferences. Required modifications were also performed within the mentioned analysis regions in order to avoid interferences with other compounds, such as water, which could be present in the sample gas. The developed calibration methods were tested with known concentrations of SO_2 and SO_3 to verify the accuracy of the measurements. For all experiments, the inlet and the outlet gas concentrations were measured with the FTIR analyzer. A reactor bypass line, heated to 200 °C, was used to verify the inlet concentrations of the feed gases. The homogeneous SO_2 oxidation rate in the gas phase is extremely low, with SO_2 conversion due to the homogeneous reaction neglected at temperatures below 900 °C [29]. In our experiments, all conversion calculations were done with respect to the measured bypass concentrations.

2.2. Catalyst pretreatment and reactor experiments

Progressive degradation of Pt/Al_2O_3 catalyst performance due to exposure to sulfur has been reported in the literature [3]. Catalyst deactivation in the presence of sulfur can occur through active metal site blocking [30,31] or support sulfation [31–33]. Changes in catalyst morphology, structure and electronic properties have been observed after sulfur exposure [32,34]. Olsson and Karlsson investigated the effect of long time SO_2 exposure to Pt, and Pt migration and sintering were observed even at temperatures as low as 200 °C [5]. Slow activity changes were also noticed during the course of this study and data obtained from temperature programmed desorption (TPD) experiments (data not shown for brevity) demonstrated a significant amount of S uptake by the support material, with a slow approach to saturation. Based on the above observations, to attain reproducibility, an overnight SO_2 exposure, 50 ppm SO_2 in N_2 at 240 °C overnight, was used as a pretreatment method except for the reaction order experiments which were conducted with a different pretreatment method (as described later in this section). The reproducibility of the data was within ±4% using the long time SO_2 exposure pretreatment. All the experiments as well as the pretreatments were conducted with total flow rate of 4.60 L/min corresponding to the space velocity of 25,000 h^{-1}.

The apparent SO_2 oxidation over $Pt/\gamma\text{-}Al_2O_3$ activation energy was determined. In the first set of experiments, the feed concentrations were varied between 100 and 149 ppm for SO_2, 54–106 ppm for SO_3 and 6–10% for O_2. It is worth mentioning that while our initial goal was to address the feed concentrations seen in diesel engine exhaust, SO_2 and SO_3 concentrations larger than normal were employed to accelerate the time to reach steady state. SO_3 was also included in the feed to maintain differential conditions within the reactor. High SO_3 levels might also be expected at the catalyst outlet under high rate conditions. Three sets of feed compositions were selected from the above ranges and the apparent activation energy was measured by randomly varying the temperature between 240 and 308 °C while keeping the feed composition constant. Another set of experiments was performed with no SO_3 in the feed to study the effect of SO_3 on the activation energy. With no SO_3 in the feed, the differential assumption for the reactor may not be as accurate as when SO_3 is present in the feed, however, in the former case, the measurements were performed multiple times while restricting data points to conversion below 10% to ensure the accuracy of the estimated value.

Global reaction orders with respect to SO_2, O_2 and SO_3 were estimated. For reaction order experiments, the catalyst sample was pretreated at 430 °C in N_2 for 30 min, rather than the long-time SO_2 exposure, with reproducible results still obtained. To minimize the effect of temperature gradients and to avoid mass transfer limitations due to concentration gradients, the reactor was operated in a differential reactor regime by restricting the SO_2 conversions to below 15%. Excess SO_3 was used in the feed to ensure the reactor operates in a differential manner. The data were recorded when steady state was reached, which typically occurred after about 1 h. Due to the transient nature of the adsorption/desorption processes over the catalyst surface, a true steady state might not be achieved during this time, especially for the low temperature data points. However, the SO_2 oxidation activity did not change significantly after collecting the steady state data points (i.e. the SO_2 concentration change was less than 1–2 ppm) and therefore the data can still be considered at steady state. In order to determine the reaction orders, the concentrations of various species were varied independently between 52 and 310 ppm for SO_2, 58–259 ppm for SO_3 and 5–15% for O_2, all at 274 °C. A power law expression was assumed for the reaction rate dependency on the SO_2, O_2 and SO_3 concentrations. The estimated values for the reaction orders, as well as the activation energy, and their standard errors were obtained by a log-linear analysis. To observe the effect of SO_3 presence in the reaction mixture, the reaction orders with respect to SO_2 and O_2 were also obtained with no SO_3 in the feed. All kinetic experiments were repeated to verify reproducibility of the data.

For the kinetic model development, the first step consisted of collecting the experimental data over the intended concentration and temperature ranges. The SO_2 and SO_3 concentrations in the feed were varied between 49–157 and 0–113 ppm, respectively, and 5–13% was used for oxygen. The data were collected between 239 and 371 °C, which is in line with the SO_2 light off temperature range over the catalyst used. More experimental data points were also taken in the higher temperature region, which is limited by thermodynamic equilibrium. Different combinations of feed concentrations and reactor temperatures were selected within the defined domain and the data were collected at randomly selected combinations—i.e. not in any concentration or temperature order.

Pt dispersion was measured using a chemisorption technique described by Karakaya et al. [35]. It is based on temperature programmed desorption (TPD) of pre-adsorbed CO in a continuous flow reactor at atmospheric pressure. Prior to the TPD experiment, a catalyst pretreatment was carried out according to the procedure described in [35]. 0.5 vol.% CO diluted in N_2 was metered to the reactor at room temperature to saturate the metal surface. The CO flow was stopped after saturation of the sample and the physisorbed CO was removed by flowing N_2 over the catalyst at room temperature. These processes were conducted with a total flow rate of 1 Std L/min. The flow rate was then decreased to 0.5 Std L/min and the TPD was performed with a heating rate of 25 °C/min from room temperature to 515 °C under continuous N_2 flow. The desorbed amounts of CO and CO_2 were obtained. The metal dispersion was calculated by assuming that all desorbed C species, i.e. CO and CO_2, originated from the adsorbed CO. Furthermore, adsorption stoichiometry of CO/Pt and CO_2/Pt were assumed to be unity. A Pt dispersion of 5.84% was obtained for the catalyst sample. Such a small dispersion was caused by thermal aging due to catalyst exposures to high temperatures (i.e. 730 °C) during multiple cycles of SO_2 TPD/TPO prior to any experiments. This cycling was done to ensure no further degradation during the experiments done in this study.

3. Modeling

The kinetics development methodology typically involves solving an outer problem and a corresponding inner problem. The outer problem is the optimization which starts with the assumption of a desired reaction rate expression along with initial guesses for the rate parameters, and changing the same to minimize the error between experimental observations and the calculated values. The corresponding inner problem involves generating exit concentrations for each set of reaction rate parameters specified by the outer problem. We begin this section by detailing the equations we

employed for solving the exit concentrations of the desired species across the reactor.

3.1. Inner problem

The equations which define the gas and surface concentrations of the species whose concentrations appreciably change across the length of the reactor are shown below. The definitions of the variables involved in these equations are detailed in the nomenclature section.

$$\frac{w}{A}\frac{\partial x_g}{\partial z} = -k_{m,i}S(x_g - x_s) = \sum_{j=1}^{nrct} a_j s_{ij} r_j \quad (1)$$

$$\frac{\partial \vec{\theta}}{\partial t} = F(r_j, \vec{\theta}, \vec{c}_s) \quad (2)$$

In the above equations, isothermal conditions for the reactor were assumed, which was also verified via temperature measurements at different positions inside the monolith, where the temperature difference was always within 3–4 °C. In addition, it was assumed that the surface temperature was the same as that in the gas and the inlet temperature defined the overall reactor temperature thus allowing $T_g = T_s = T_{in}$. To further simplify the overall problem and focus on the task of developing reaction kinetics on the surface, several assumptions were made in the mass balance equations (i.e. Eqs. (1) and (2)). First, since steady-state conversion data were used, it was assumed that there were no transients. Second, it was assumed that mass transfer is reasonably fast compared to the reaction rates. This assumption was verified by calculating the Weisz-Prater number and Mear's criteria for the internal and external mass transfer limitations, respectively. The equations described above will then transform to the form:

$$\frac{w}{A}\frac{dx_g}{dz} = \sum_{j=1}^{nrct} a_j s_{ij} r_j \quad (3)$$

where x is the mole fractions of species $i = SO_2$ or SO_3 and:

$$0 = \vec{F}(r_j) \quad (4)$$

where $\vec{F}$ is the governing equation of each coverage site. The set of equations constitutes a differential algebraic equation (DAE) system and was solved using ode15s in Matlab. The activation energies were scaled as reported previously [28] to increase robustness. Via this approach, surface coverages and species exit concentrations are provided, which in turn were used by the outer problem to perform the desired optimization.

3.2. Outer problem

A reaction rate scheme is needed before optimizing rate parameters against experimental data. A reaction mechanism previously reported by Dawody et al. [11] was assumed. For the oxidation of SO_2 on the Pt surface, they proposed a Langumuir-Hinshelwood based mechanism. The same mechanism was adopted for this study, and their rate parameters were used as initial guesses for the optimization. The adopted Langmuir-Hinshelwood model is:

$$SO_2(g) + Pt \overset{1,2}{\longleftarrow} Pt\text{-}SO_2 \quad (5)$$

$$O_2(g) + 2Pt \overset{3,4}{\longleftarrow} 2Pt\text{-}O \quad (6)$$

$$Pt\text{-}SO_2 + Pt\text{-}O \overset{5,6}{\longleftarrow} Pt\text{-}SO_3 + Pt \quad (7)$$

$$Pt\text{-}SO_3 \overset{7,8}{\longleftarrow} SO_3(g) + Pt \quad (8)$$

Table 1
Initial value of the kinetic parameters from Dawody et al. [11].

Parameter	Initial value	Parameter	Initial value (kJ mol^{-1})
A_1	4.8×10^7 m^3 mol^{-1} s^{-1}	E_1	7
A_2	1×10^{15} s^{-1}	E_2	150
A_3	8.44×10^5 m^3 mol^{-1} s^{-1}	E_3	10.40
A_4	9.97×10^{14} s^{-1}	E_4	189.40
A_5	6.4×10^{14} s^{-1}	E_5	179
A_6	6.2×10^{15} s^{-1}	E_6	182
A_7	1×10^{15} s^{-1}	E_7	140
A_8	4.7×10^7 m^3 mol^{-1} s^{-1}	E_8	4

The objective function used for optimization is adopted from Sampara et al. [28].

$$f^2 = \frac{1}{n_T}\sum_{j=1}^{n_T}\frac{1}{n_j}\sum_{j=1}^{n_j}\log^2\left(\frac{X_{SO_2}^{model}}{X_{SO_2}^{expt}}\right) \quad (9)$$

where X_{SO_2} is the SO_2 conversion at the reactor outlet, n_T is the number of temperatures included in the experimental data set and n_j is the number of points at each temperature. Since the experimental conversions used did not include high conversion data, we defined the objective function based on conversions and not on the combination of conversions and exit concentrations as previously reported in [28]. Matlab's constrained optimizer, called fmincon, was utilized for the optimization process. To identify the parameters requiring adjustment for a match to the experimental data, a sensitivity analysis was performed. Thermodynamic consistency of the kinetic parameters was also considered in the fitting procedure.

The initial guesses for the activation energies and pre-exponential factors for the various reactions were obtained from Dawody et al. [11] and are listed in Table 1 for comparison. All the pre-exponential factors given here are based on the molar amount of active sites. During model implementation, however, the pre-exponential factors were multiplied by the molar amount of active sites per kg of catalyst. For example, the unit of the pre-exponential factor for the adsorption steps is given as m^3 mol^{-1} s^{-1} in Table 1, whereas in the model calculations it was multiplied by the exposed Pt site density and therefore converted to m^3/(kg catalyst s).

4. Results and discussion

4.1. Reaction kinetics measurements

The overall rate of reaction for SO_2 oxidation can be written in a power law form as follows:

$$r = A\exp\left(\frac{-E_a}{RT}\right)[SO_2]^a[O_2]^b[SO_3]^c(1-\beta_{eq}) \quad (10)$$

where A is the frequency factor for the forward rate constant, E_a the activation energy, $[SO_2]$, $[O_2]$ and $[SO_3]$ are the gas-phase concentrations of SO_2, O_2 and SO_3, respectively, a, b and c are the forward reaction orders, and β_{eq} is the approach to equilibrium and defined as:

$$\beta_{eq} = \frac{[SO_3]}{[SO_2][O_2]^{0.5}K_{eq}} \quad (11)$$

with K_{eq} the equilibrium constant of the overall reaction. The apparent activation energy was calculated based on the experimental data obtained in the presence and absence of SO_3 in the feed. The temperature dependence of the SO_2 oxidation turnover rate (TOR) for experiments with and without SO_3 in the feed is shown in Fig. 1 where the TORs represent the observed reaction rates. The high temperature data were not used in the activation energy calculations, therefore the equilibrium term, i.e. β_{eq}, was small enough to be neglected and the observed TORs approximately represent the forward reaction rates. The SO_2 conversions used in the TOR

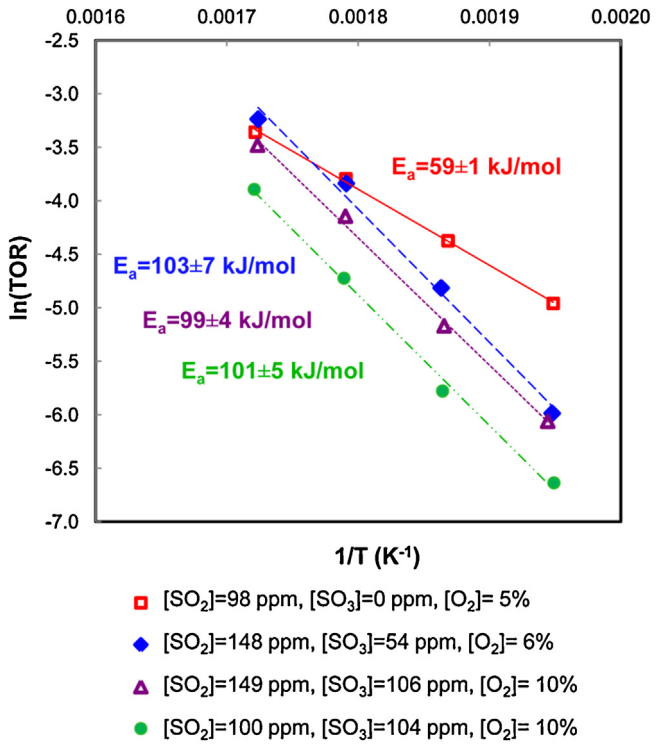

Fig. 1. Arrhenius plot for SO_2 oxidation on Pt/γ-Al_2O_3 in the presence and absence of SO_3 in the feed.

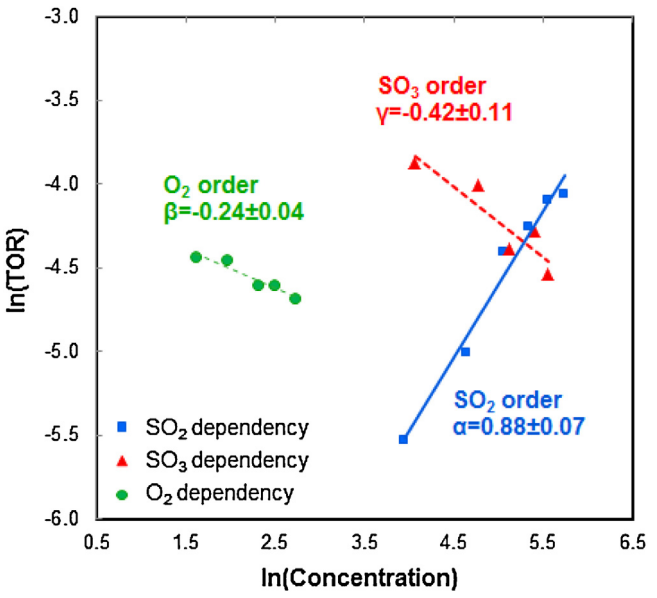

Fig. 2. SO_2 Oxidation TOR dependence on SO_2, O_2 and SO_3 concentrations at 274 °C. Feed for SO_2 order: 52–310 ppm SO_2, 10% O_2, 169 ppm SO_3;feed for SO_3 order:208 ppm SO_2, 10% O_2, 58–259 ppm SO_3; feed for O_2 order: 208 ppm SO_2, 5-15% O_2, 167 ppm SO_3. All feeds have N_2 as the balance gas.

calculations were all obtained using the SO_2 concentration measured at the inlet and outlet of the reactor, with a SO_2 measurement error within 1 ppm. An apparent activation energy of 59 ± 1 kJ mol^{-1} was obtained with no SO_3 in the feed, whereas an activation energy of 101 ± 3 kJ mol^{-1} was calculated with SO_3 in the feed, indicating that SO_3 inhibits the SO_2 oxidation rate. The values of the activation energy obtained for different feed concentrations are shown in Fig. 1. The observed inhibition effect for SO_3 is similar to the NO_2 inhibition effect on the NO oxidation rate over Pt as widely reported in the literature [36–38].

Reaction order experiments were performed in the differential reactor regime with conversions below 15% and β_{eq} values below 0.0004, demonstrating that the reaction was far from equilibrium. The first set of experiments was done with no SO_3 in the feed and the forward reaction orders were determined using a least squares analysis. The results of these experiments are summarized in Table 2. In order to investigate the effect of SO_3, another set of experiments was performed with SO_3 added to the feed and reaction orders again calculated, again with data listed in Table 2. In this case the SO_2 reaction order was 0.88 and −0.24 for O_2, similar to those obtained in the absence of SO_3 in the feed. The SO_3 reaction order was calculated as −0.42, demonstrating its inhibition effect. Fig. 2 shows the effects of reactant and product concentrations on the observed SO_2 oxidation TOR at 274 °C with SO_3 as part of the feed. In order to examine the effect of operating conditions on the reaction rate dependencies, a number of experiments were performed using different feed concentrations and temperatures, all within the differential reactor regime, and reaction orders similar to those reported in Table 2 were obtained.

Table 2
Experimental reaction orders for SO_2 oxidation on Pt/γ-Al_2O_3.

Experiment	SO_2 order	SO_3 order	O_2 order
With no SO_3 in the feed	0.72 ± 0.15	–	-0.22 ± 0.12
With SO_3 in the feed	0.88 ± 0.07	-0.42 ± 0.11	-0.24 ± 0.04

4.2. Kinetic model results

The system of differential algebraic equations was solved at different temperatures to predict the steady-state SO_2 conversion as well as the coverage of the adsorbed species along the monolith length. A set of experimental data measured within the defined domains of the feed concentration and temperature, as described in Section 2.2, was used in order to optimize the kinetic parameters. To ensure that the model satisfies thermodynamic equilibrium, some data points in the high temperature region were also added to the optimization data set. To minimize the effect of measurement errors, the SO_2 concentrations at the inlet and outlet of the reactor were considered and any data point with a concentration change smaller than 8 ppm was dropped from the experimental data set. It needs to be mentioned again that the SO_2 measurement error is within 1 ppm according to the FTIR calibration. Therefore, the arbitrarily chosen 8 ppm margin overestimates the experimental error simply in order to decrease the uncertainty of the adjusted parameters. It also accounts for any experimental errors other than those related to the FTIR calibration, such as possible deviations from a true steady state. Ultimately, 31 data points were employed for the parameter estimation as listed in Table 3. The data points added to the experimental data set in the high temperature region, representing the equilibrium-controlled reaction, are not included in Table 3 for brevity. It should be noted that the equilibrium constraint has already been considered in the parameter estimation within the model, therefore the equilibrium data are only used to double check model consistency under equilibrium-limited conditions and they have no further effect on the fitting of the kinetic parameters. Sensitivity analysis shows that the model is sensitive to the kinetic parameters of oxygen adsorption/desorption (steps 3 and 4) as well as the surface reaction (steps 5 and 6). Indeed, the kinetic parameters related to the SO_2 and SO_3 adsorption/desorption steps did not have a significant effect on the model predictions. This is consistent with the rate determining step evaluation, discussed later in this section. To keep the number of adjustable parameters as low as possible, only the activation energies of steps 3–6 were optimized and the pre-exponential

Table 3
Experimental data used for parameter optimization (the data in the equilibrium controlled region are not listed here). Total flow rate for all data points is 4.60 L/min.

No.	Inlet temperature (°C)	Inlet concentrations			Exit SO_2 conversion (%)
		SO_2 (ppm)	SO_3 (ppm)	O_2 (%)	
1	239	98	5	5	12%
2	250	98	8	10	14%
3	260	99	54	10	9%
4	261	98	6	5	22%
5	261	98	28	10	11%
6	261	148	53	6	9%
7	282	150	107	13	16%
8	283	148	56	6	25%
9	283	99	52	6	22%
10	283	50	104	7	19%
11	283	99	54	10	20%
12	283	98	29	10	26%
13	283	51	103	10	18%
14	283	100	76	10	18%
15	283	98	8	10	37%
16	283	100	105	10	15%
17	283	98	6	5	39%
18	295	100	53	13	21%
19	305	148	55	6	45%
20	305	50	104	10	40%
21	305	100	105	10	35%
22	305	98	6	5	61%
23	306	50	102	7	41%
24	316	98	8	10	48%
25	317	98	8	10	65%
26	327	100	79	10	68%
27	327	50	102	7	71%
28	327	98	6	5	81%
29	327	148	55	6	71%
30	350	98	6	5	95%
31	372	98	6	5	100%

factors were kept constant. To maintain the thermodynamic consistency of the model, the activation energy for SO_2 desorption (step 2) was calculated based on thermodynamic restrictions. Thermodynamic constraints include the enthalpic and entropic terms. To satisfy the enthalpic constraint, the enthalpy change resulting from the individual activation energies is equal to the overall reaction enthalpy. The entropic constraint was already satisfied as the original set of pre-exponential factors was thermodynamically consistent and they were not changed in the optimization. The values of the pre-exponentials as well as the rest of the activation energies, which were constant during the optimization, were the same as those listed in Table 1. The optimization was performed by minimizing the objective function given in Eq. (9) using Matlab. The values of the optimized kinetic parameters are listed in Table 4. The optimized parameters were used in the kinetic model and the SO_2 conversions under different experimental conditions were predicted. The model-predicted and experimental conversions are compared in a parity plot shown in Fig. 3.

The steady-state SO_2 oxidation model was validated using a set of experimental data which was not included in the optimization procedure. The model prediction for this experiment is shown in Fig. 4. As can be observed, the model with the optimized parameters is able to accurately predict the experimental data. Since SO_2 oxidation is an exothermic reaction, conversion at high temperatures is limited by thermodynamic equilibrium. In fact, the experimental data in the high temperature region consistently met the equilibrium curve. Therefore, instead of taking more data points at high temperature region, the model accuracy in this region was examined by comparing the predicted conversion with the equilibrium conversion obtained from Gibbs free energy calculations. Variations of the equilibrium constant with temperature are related to the reaction Gibbs free energy according to the following expression:

$$K_{eq} = \exp\left(-\frac{\Delta G}{RT}\right) \quad (12)$$

where ΔG is the Gibbs free energy of SO_2 oxidation, which is a function of temperature, R the gas constant and T is the temperature. The equilibrium constant, i.e. K_{eq}, is also related to the conversion

Table 4
Optimized value of the kinetic parameters.

Parameter	Optimized value (kJ mol^{-1})
E_2	128.3[a]
E_3	11.2
E_4	184.7
E_5	153.4
E_6	180.1

[a] Calculated from thermodynamic restrictions.

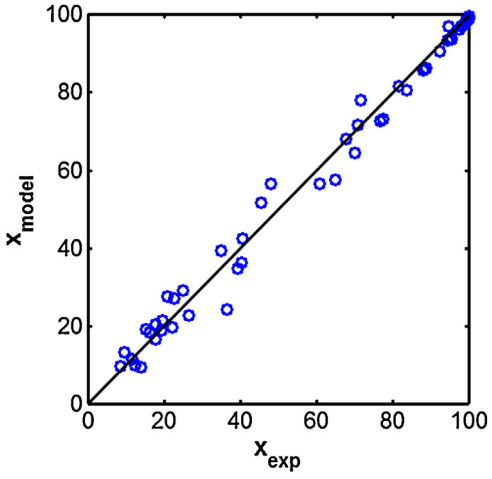

Fig. 3. Comparison between experimental and model-predicted conversions.

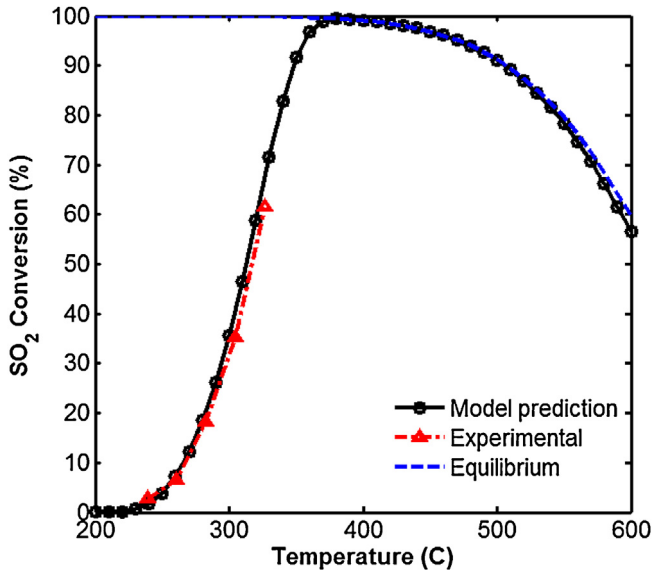

Fig. 4. SO_2 conversion as a function of temperature, model predictions and experimental data are shown along with equilibrium-limited conversion at high temperatures. Feed composition: 149 ppm SO_2, 10% O_2 and 106 ppm SO_3.

according to its definition. Therefore, equilibrium conversion can be calculated as a function of temperature using Eq. (12).

The relative importance of each step in the reaction mechanism was studied at different temperatures to identify the rate determining step. The optimized kinetic parameters were used in the microkinetic model and the system of differential algebraic expressions was solved at four different temperatures. At each temperature, the rate of individual steps was calculated and integrated along the length of the monolith, thus an average rate was obtained for each of the eight steps in the reaction mechanism. The average rates were then compared in the bar chart shown in Fig. 5. It should be noted that the forward and backward reaction steps in the Langmuir-Hinshelwood mechanism, i.e. Eqs. (5)–(8), are separated as individual steps in the rate calculations. However, since the reaction pairs are important for the overall SO_2 oxidation, they are

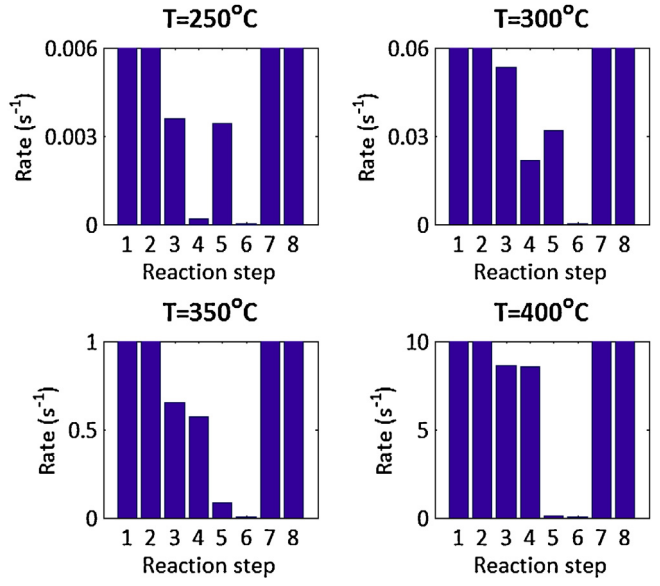

Fig. 5. Comparison between the rates of individual steps in the mechanism at different temperatures; in case of O_2 adsorption/desorption, the values of $2r_3$ and $2r_4$ are plotted. Feed composition: 149 ppm SO_2, 10% O_2 and 106 ppm SO_3.

Table 5
Average rates for each step at different temperatures, the rate unit is s^{-1}.

Temperature (°C)	250	300	350	400
r_1	3.58	1.12×10^{1}	1.74×10^{1}	1.42×10^{1}
r_2	3.57	1.12×10^{1}	1.73×10^{1}	1.41×10^{1}
$2r_3$	3.57×10^{-3}	5.33×10^{-2}	6.55×10^{-1}	8.62
$2r_4$	1.63×10^{-4}	2.16×10^{-2}	5.73×10^{-1}	8.53
r_5	3.41×10^{-3}	3.18×10^{-2}	8.23×10^{-2}	9.87×10^{-2}
r_6	3.49×10^{-7}	1.24×10^{-5}	3.94×10^{-4}	1.01×10^{-2}
r_7	5.19	2.29×10^{1}	1.12×10^{2}	4.62×10^{2}
r_8	5.19	2.29×10^{1}	1.12×10^{2}	4.62×10^{2}

considered as a pair of forward/backward steps in the RDS analysis. The RDS can be found by comparing the contribution of an individual step reaction rate to the overall rate. One approach is to evaluate the ratio of the forward rate of step i to the overall rate, i.e. $r_i^+/r_{overall}$, and when equal to 1, then this step is rate determining [39]. Based on Fig. 5, it appears that O_2 adsorption/desorption and/or the surface reaction could be rate determining.

Under steady state conditions, the time derivative will be zero, thus the net rate of O_2 adsorption/desorption, i.e. $2(r_3 - r_4)$, is equal to the net rate of surface reaction, i.e. $(r_5 - r_6)$, etc. with all reaction pair net rates equal:

$$r_{overall} = r_1 - r_2 = 2(r_3 - r_4) = r_5 - r_6 = r_7 - r_8 \quad (13)$$

Note, when comparing the forward rates with the overall rate, the stoichiometric coefficient for the O_2 adsorption/desorption step, 1/2, can be considered. Therefore, in Fig. 5 and Table 5, where the individual rate values are compared, the rate values for this step are represented as $2r_3$ and $2r_4$, rather than r_3 and r_4.

As observed in Fig. 5, the SO_2 and SO_3 adsorption/desorption steps (steps 1, 2 and 7, 8) are fast compared to O_2 adsorption/desorption and the surface reaction steps over the entire temperature range studied. The rate values for the four rapid reactions are well above the y axis limits shown in Fig. 5, with an order of magnitude larger than one, and are truncated such that the values of the rate for steps 3 to 6 can be compared easily. The values of the average rates for each step calculated at the four different temperatures are listed in Table 5. As can be seen in the top panels of Fig. 5, at the two low temperatures characterized, i.e. 250 and 300 °C, oxygen adsorption and surface reaction are slow compared to the other forward steps, which are important for the progress of the overall reaction. Therefore, the overall reaction is controlled by both oxygen adsorption/desorption and surface reaction at temperatures below 300 °C, while the other steps are significantly faster and can be assumed to be quasi-equilibrated. As temperature increases, oxygen adsorption/desorption becomes faster whereas the forward and backward surface reactions are still significantly slower than the other steps. Therefore, as can be observed in the two bottom panels of Fig. 5, the surface reaction is the only rate limiting step at temperatures above 300 °C. The modeling results therefore suggest that the SO_2 oxidation kinetics are sensitive to both oxygen adsorption/desorption and surface reaction at temperatures below 300 °C, whereas at higher temperatures, the surface reaction is the rate limiting step.

This result differs from that which Benzinger et al. [17] reported in their study, where SO_2 adsorption was determined as the rate limiting step, under high concentrations of SO_2. It could be due to the quite different operating conditions under which SO_2 oxidation has been studied. The sensitivity of the RDS to the temperature range, suggested in the present study, confirms their conclusion regarding the possibility of different rate limiting steps depending on the experimental conditions.

The predicted surface coverages of adsorbed SO_2, SO_3 and oxygen as a function of monolith length at three different temperatures are shown in Fig. 6. These coverages were calculated using the

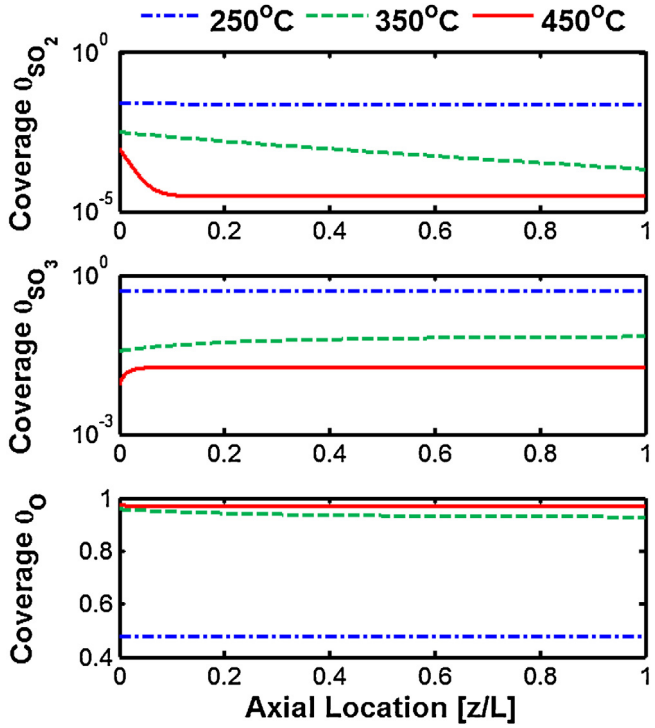

Fig. 6. Calculated surface coverages along the monolith channel at three different temperatures. Feed composition: 149 ppm SO_2, 10% O_2 and 106 ppm SO_3.

kinetic model with the same feed composition used in Fig. 4. As shown in the first panel of Fig. 6, the adsorbed SO_2 has the smallest coverage on the Pt surface at all three temperatures. At 250 °C, the Pt sites are mostly covered with adsorbed SO_3 and oxygen with approximately equal contributions. As temperature increases, the SO_3 coverage decreases and oxygen becomes dominant on the Pt surface. These changes can be seen more clearly in Fig. 7 where the coverages at the channel outlet are plotted as a function of temperature. Since under these conditions the coverages do not change significantly along the monolith channel, the outlet coverage can

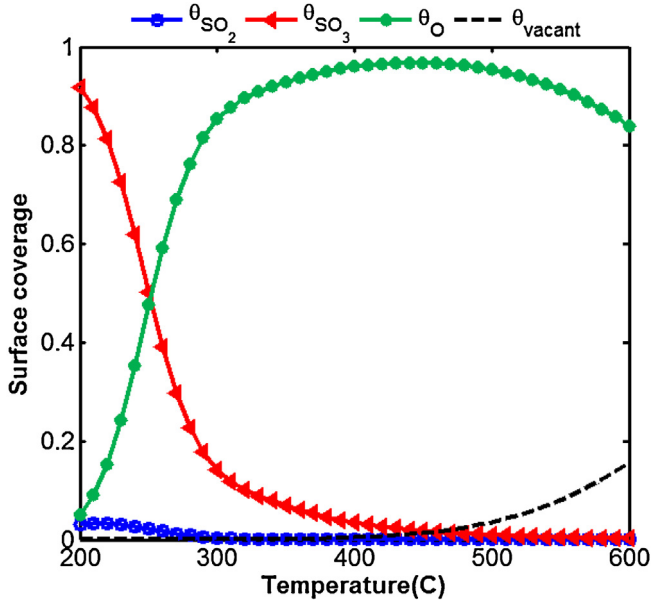

Fig. 7. Surface coverages calculated at the channel outlet as a function of temperature. Feed composition: 149 ppm SO_2, 10% O_2 and 106 ppm SO_3.

properly represent the coverage inside the channel. The model predicts oxygen as the most abundant surface intermediate (MASI) at temperatures above 300 °C. The oxygen coverage starts to decrease at temperatures above 500 °C where the density of the vacant sites increases.

These results can be explained based on the relative importance of the individual steps at different temperatures. With SO_3 present in the feed, a large fraction of the active sites are occupied by the adsorbed SO_3 at temperatures below 300 °C, inhibiting the progress of the overall reaction. In the case of no SO_3 in the feed, since the reverse surface reaction is slow, some amount of produced SO_3 could still remain on the surface, especially in the downstream portion of the catalyst, with a smaller degree of SO_3 inhibition. At higher temperatures, O_2 adsorption/desorption becomes faster compared to the forward/backward surface reaction, with surface reaction being the RDS. It has been widely reported in the literature that oxygen is the most abundant surface intermediate on the Pt surface for both NO oxidation [38] and SO_2 oxidation [11,17]. For SO_2 oxidation on Pt, such an assumption is not true at all temperatures as the modeling results suggest that the oxygen coverage as well as other surface coverages are strongly dependent on reaction temperature and feed composition.

The model predictions also agree with the higher activation energy observed in the presence of SO_3 in the feed. As described in Section 4.1, the activation energy measurements were performed in the 240–308 °C temperature range where, according to the model, both O_2 adsorption/desorption and surface reaction are important for the progress of the overall reaction. This implies that SO_3 inhibits SO_2 oxidation through occupation of the active sites required for oxygen adsorption, leading to a slower oxidation rate in the low temperature region. This result is confirmed with the high coverage of SO_3 predicted by the model at low temperatures. Data also show that, as SO_3 increases in concentration, its inhibition effect is nonlinear, and increases in inhibition extent become less significant with increasing levels of SO_3 in the feed. This is also consistent with SO_3 inhibition through competitive adsorption on Pt sites, since as the concentration increases, some level of a saturation effect will occur.

Consistency of the model prediction with the observed reaction orders was also examined using global rate analysis for the proposed Langmuir-Hinshelwood mechanism. In taking the standard approach, each of the four reaction steps were assumed rate limiting, with the other three at equilibrium. This leads to the derivation of four global rate equations for comparison. The experimental reaction orders measured are consistent, with certain key assumptions, with global rate expressions derived assuming either SO_2 adsorption/desorption or the surface reaction as the RDS. Since the latter is predicted as the RDS within a wide temperature range via the microkinetic model, the results of our analysis for this case are presented here. The following rate expression is obtained assuming the surface reaction to be the RDS:

$$-r_{SO_2} = \frac{k_5(k_1/k_2)\sqrt{k_3/k_4}\,[SO_2]\,[O_2]^{1/2}}{1+(k_1/k_2)\,[SO_2]+\sqrt{k_3/k_4\,[O_2]}+k_8/k_7\,[SO_3]}(1-\beta_{eq}) \quad (14)$$

Based on the optimized kinetic parameters and the species concentrations employed in this study, the first and second terms in the denominator are negligible compared to the other terms in the whole temperature range studied. Therefore, the global rate expression can be simplified to

$$-r_{SO_2} = \frac{k_5(k_1/k_2)\sqrt{k_3/k_4}\,[SO_2]\,[O_2]^{1/2}}{\sqrt{k_3/k_4\,[O_2]}+(k_8/k_7)\,[SO_3]}(1-\beta_{eq}) \quad (15)$$

where the first and second terms in the denominator represent the oxygen and SO_3 coverages, respectively. This Eq. (15) suggests that the SO_2 oxidation reaction is first order with respect to SO_2 and negative order with respect to SO_3, consistent with our experimental reaction orders. In the low temperature region, the order of magnitude of both terms in the denominator are comparable, verifying the importance of oxygen and SO_3 coverages. The rate dependency on oxygen is weak at such low temperatures, again in line with the observed reaction orders. At higher temperatures, the first term in the denominator becomes larger, indicating a higher contribution of oxygen coverage on the surface, resulting from the faster O_2 adsorption/desorption step.

5. Conclusions

SO_2 oxidation was studied over a Pt/γ-Al_2O_3 oxidation catalyst. Experimental measurements were used to calculate an apparent activation energy of 101 kJ mol^{-1}. Reaction orders of 0.88 and −0.24 were determined with respect to SO_2 and O_2, respectively, and the SO_3 reaction order was −0.42, demonstrating its inhibition effect. A microkinetic model based on a Langmuir-Hinshelwood mechanism was proposed for the catalytic oxidation of SO_2 on Pt/γ-Al_2O_3 and a one-dimensional steady-state model was developed for a single channel of a monolith. A set of kinetic parameters, taken from the literature [11], was used in solving the reactor model, with some parameters optimized to match the experimental data. A separate set of experimental data, which was not included in the parameter optimization, was used to validate the kinetic model. The developed model was able to accurately predict the experimental behavior of the catalyst. The model predicts that oxygen adsorption/desorption and surface reaction control the overall rate at temperatures below 300 °C. As temperature is increased, oxygen adsorption/desorption more rapidly increases relative to the surface reaction between the adsorbed SO_2 and oxygen, which becomes the only RDS at temperatures above 300 °C. The modeling results revealed that at low temperatures, i.e. 200 °C, the adsorbed SO_3 had the highest coverage on the Pt surface followed by oxygen and SO_2. However, as temperature increases, the adsorbed oxygen becomes the most abundant surface intermediate, consistent with literature results [11,17]. The modeling results also revealed that the relative importance of the individual rates in the mechanism as well as the surface coverages were strongly dependent on temperature. Global rate analysis, assuming the surface reaction as the RDS, verifies the results of our microkinetic model with a rate expression consistent with the experimental reaction orders.

Acknowledgements

The authors gratefully acknowledge Cummins Inc. for financial support and Johnson Matthey for the donated catalyst sample.

References

[1] J.Y. Luo, D. Kisinger, A. Abedi, W.S. Epling, Appl. Catal. A: Gen. 383 (2010) 182–191.
[2] E. Xue, K. Seshan, J. Ross, Appl. Catal. B: Environ. 11 (1996) 65–79.
[3] A. Russell, C. Henry, N.W. Currier, A. Yezerets, W.S. Epling, Appl. Catal. A: Gen. 397 (2011) 272–284.
[4] O. Krocher, M. Widmer, M. Elsener, D. Rothe, Ind. Eng. Chem. Res. 48 (2009) 9847–9857.
[5] L. Olsson, H. Karlsson, Catal. Today 147S (2009) S290–S294.
[6] J.H. Pazmiño, J.T. Miller, S.S. Mulla, W.N. Delgass, F.H. Ribeiro, J. Catal. 282 (2011) 13–24.
[7] J.M. Jones, V.A. Dupont, R. Brydson, D.J. Fullerton, N.S. Nasri, A.B. Ross, A.V.K. Westwood, Catal. Today 81 (2003) 589–601.
[8] F. Zhong, Y. Zhong, Y. Xiao, G. Cai, Y. Zheng, K. Wei, Chin. J. Catal. 32 (2011) 1469–1476.
[9] L. Olsson, M. Fredriksson, R.J. Blint, Appl. Catal. B: Environ. 100 (2010) 31–41.
[10] J. Dawody, M. Skoglundh, L. Olsson, E. Fridell, J. Catal. 234 (2005) 206–218.
[11] J. Dawody, M. Skoglundh, L. Olsson, E. Fridell, Appl. Catal. B: Environ. 70 (2007) 179–188.
[12] A. Urbanek, M. Trela, Catal. Rev. Sci. Eng. 21 (1) (1980) 73–133.
[13] K.C. Xie, J.A. Nobile, J. Catal. 94 (1985) 323–334.
[14] J.L. Sorensen, H. Livbjerg, J. Villadsen, Chem. Eng. Sci. 43 (8) (1988) 2269–2274.
[15] J. Svachula, L.J. Alemany, N. Ferlazzo, P. Forzatti, E. Tronconi, Ind. Eng. Chem. Res. 32 (1993) 826–834.
[16] J.P. Dunn, H.G. Stenger Jr., I.E. Wachs, Catal. Today 51 (1999) 301–318.
[17] W. Benzinger, A. Wenka, R. Dittmeyer, Appl. Catal. A: Gen. 397 (2011) 209–217.
[18] H.N. Sharma, S.L. Suib, A.B. Mhadeshwar, Interactions of Sulfur Oxides with Diesel Oxidation Catalysts (DOCs), ACS Symposium Series, Washington, DC, 2013.
[19] S. Astegger, E. Bechtold, Surf. Sci. 122 (1982) 491–504.
[20] U. Kohler, H. Wassmuth, Surf. Sci. 126 (1983) 448–454.
[21] M. Polcik, L. Wilde, J. Haase, B. Brena, G. Comelli, G. Paolucci, Surf. Sci. 381 (1997) L568–L572.
[22] K. Wilson, C. Hardacre, C.J. Baddeley, J. Ludecke, D.P. Woodruff, R.M. Lambert, Surf. Sci. 372 (1997) 279–288.
[23] Y.M. Sun, D. Sloan, D.J. Alberas, M. Kovar, Z.J. Sun, J. White, Surf. Sci. 319 (1994) 34–44.
[24] R. Streber, C. Papp, M.P.A. Lorenz, O. Höfert, E. Darlatt, A. Bayer, R. Denecke, H.P. Steinrück, Chem. Phys. Lett. 494 (2010) 188–192.
[25] X. Lin, W.F. Schneider, B.L. Trout, J. Phys. Chem. B 108 (2004) 13329–13340.
[26] C. Suzuki, Y. Yamada, T. Nakagiri, Appl. Surf. Sci. 256 (2009) 862–869.
[27] M. Happel, N. Luckas, F. Vin, M. Sobota, M. Laurin, A. Gorling, J. Libuda, J. Phys. Chem. C 115 (2011) 479–491.
[28] C.S. Sampara, E.J. Bissett, M. Chmielewski, C.P. Blvd, Ind. Eng. Chem. Res. 47 (2008) 311–322.
[29] C. Cullis, M. Mulcahy, Combust. Flame 18 (1972) 225–292.
[30] M. Skoglundh, A. Ljungqvist, M. Petersson, E. Fridell, N. Cruise, O. Augustsson, E. Jobson, Appl. Catal. B: Environ. 30 (2001) 315–328.
[31] A. Hinz, M. Skoglundh, E. Fridell, A. Andersson, J. Catal. 201 (2001) 247–257.
[32] J.K. Lampert, M. Shahjahan, R.J. Farrauto, Appl. Catal. B: Environ. 14 (1997) 211–223.
[33] D.L. Mowery, R.L. McCormick, Appl. Catal. B: Environ. 34 (2001) 287–297.
[34] F. Cabello Galisteo, R. Mariscal, M. López Granados, M.D. Zafra Poves, J.L.G. Fierro, V. Kröger, R.L. Keiski, Appl. Catal. B: Environ. 72 (2007) 272–281.
[35] C. Karakaya, O. Deutschmann, Appl. Catal. A: Gen. 445–446 (2012) 221–230.
[36] S.S. Mulla, N. Chen, W.N. Delgass, W.S. Epling, F.H. Ribeiro, Catal. Lett. 100 (3–4) (2005) 267–270.
[37] S.S. Mulla, N. Chen, L. Cumaranatunge, G. Blau, D. Zemlyanov, W.N. Delgass, W.S. Epling, F.H. Ribeiro, J. Catal. 241 (2006) 389–399.
[38] D. Bhatia, R.W. McCabe, M.P. Harold, V. Balakotaiah, J. Catal. 266 (2009) 106–119.
[39] J.A. Dumesic, D.F. Rudd, L.M. Aparicio, J.E. Rekoske, A.A. Trevino, The Microkinetics of Heterogeneous Catalysis, ACS Professional Reference Book, Washington, DC, 1993.